Chemical Enrichment of Spiral Galaxies: Metallicity-Luminosity Relation

M. Mollá

Abstract Elemental abundances increased very rapidly at the early times of evolution of galaxies. Therefore, to interpret the high redshift observations by using synthesis models without taking into account the chemical evolution may yield erroneous conclusions. We will show how spiral and irregular galaxies evolve using a grid of realistic chemical and spectrophotometric models, able to reproduce the galaxies data of our local universe. By using these calibrated models, we may study a possible evolution of the metallicity-luminosity relation, such as other galaxy data correlation,s with the redshift.

1 Introduction

One of the questions arising when high redshift object data are obtained is if the classical luminosity-metallicity relation maintains its vality and continues with the same slope or not, or if, on the contrary, it evolves and changes with the redshift.

In order to analyze the high redshift data related with this one and other relationships, where photometric and chemical evolution quantities are used, we need to utilize realistic evolutionary models applied to spiral and irregular galaxies. It means that these models must be able to reproduce the local galaxies characteristics before to be used to interpret high redshift data.

Other important point resides in the spatial and time resolution of these models. The first one implies to take into account the existence of radial gradients of elemental abundances and local differences in the gas or stellar densities within spiral disks. Since we are going to compare these local quantities with other global characteristics as luminosities, it is necessary to account for these facts before to apply models, when compare the data with our expectations. It means that theoretical models must to have the adequate spatial resolution with radial distributions as results.

M. Mollá
CIEMAT, Avda. Complutense 22, 28040, Madrid (Spain) e-mail: mercedes.molla@ciemat.es

For what refers to the time resolution, it is well known that if stars formed in the 10 Myr previous to the observations, the luminosity may change strongly compared with the corresponding one of the same age and/or metallicity but without the last burst contribution. High star formation rates are expected at certain values of redshifts for spiral and irregular galaxies, and therefore we expect that observations will include a certain proportion of young stellar population contribution. Calculations must include not only the contributions of old stellar populations, but also the youngest ages stars. In the same way it is necessary to be aware that elemental abundances increase very rapidly in the firts phases of the evolution of the galaxy, and therefore, they change very much for high redshifts.

2 Chemical evolution models

We show here our results obtained for our grid of chemical evolution models [9], computed with the multiphase chemical evolution code [1, 2]. We have calculated the chemical evolution of a certain number of theoretical galaxies defined by the total mass and its radial distribution (that is, by the rotation curve and the maximum rotation velocity) by assuming different possible values for molecular cloud and star formation efficiencies. Our grid consists of 440 galaxies, with 44 different total masses (or sizes) allowing for 10 possible values of efficiencies, given by a number N from 1 (the highest value of efficiency) to 10 (the lowest one). This way we have a bi-parametric grid of models which would be represented as a plane diagram. The model corresponding to a rotation velocity Vrot= 200 km.s^{-1} and and $N = 4$ is calibrated to reproduce the Milky Way Galaxy observations, such as it has been obtained in [3, 4]. In this diagram the Hubble Sequence galaxies are located in a diagonal line, with the earliest galaxies represented by the massive objects and low values of N (that is a strong and early star formation and a low gas fraction and high abundances in the present time), while the latest galaxies are those with the lowest mass and high N's (therefore with high present star formation rate and with a large gas fraction and low metallicities). In fact, bright normal spiral and irregular galaxies, located along the Hubble Sequence, are also well fitted by different size theoretical galaxies and/or N values models (see [9] for details).

In Fig. 1, the star formation history and the age metallicity relation are represented for 4 selected models which correspond to a low and a high mass galaxy with a rotation velocity of 70 km/s and 290 km/s, respectively. For each mass radial distribution, two models, those of the highest and the lowest efficiences, are shown. We see that a low dwarf galaxy with a very low star formation efficiency has now a the maximum star formation rate, although with a very low absolute value $\sim 2.10^{-4} M_{\odot} yr^{-1}$, and therefore the age is $\tau < 2$ Gyr and the metallicity is low, $[\mathrm{Fe/H}] = -2.0$ dex, as expected for the Blue Compact Galaxies or the HII galaxies. With the same mass if the efficiency is high, N= 1, stars formed in the past, with a mean stellar age of $\tau > 8$ Gyr, showing now a relatively high metallicity $[\mathrm{Fe/H}] = +0.1$ A bright massive galaxy with N= 1 has a mean age $\tau > 12$ Gyr and

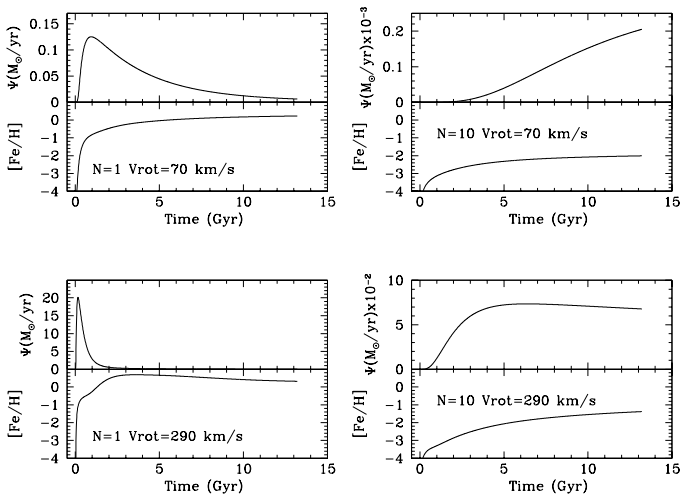

Fig. 1 Star formation and enrichment history for 4 extreme models with N=1 and 10 and rotation velocity 70 and 290 km/s, respectively, as labelled.

a high metallicity [Fe/H]$= +0.2$ dex. The same massive galaxy with N$= 10$ would have an age $\tau < 8$ Gyr and a very low metallicity [Fe/H] $= -1.4$ dex. In the first case the SFR was high in the past, ~ 20 M$_\odot$ yr^{-1}, in the second case, the SFR is almost constant from 9 Gyr ago until now, with a value of ~ 0.08 M$_\odot$ yr^{-1}.

3 Spectro-photometrical evolutionary models

We have used the new evolutionary synthesis models from [10] to obtain consistently the spectro-photometric evolution of these spiral and irregular galaxies (see [11] for more details). By using the star formation history and the age-metallicity relation obtained from the above described calculations we obtain the spectral energy distribution (SED) $F_\lambda(t)$ for each radial region of a galaxy from the deconvolution equation:

$$F_\lambda(t) = \int_0^t S_\lambda(\tau, Z)\Psi(t')dt', \tag{1}$$

where $\tau = t - t'$ and $S_\lambda(\tau, Z)$ is the SED of each Single Stellar Populations (SSP) of a given age τ and a metallicity Z. These SED are chosen between the SSPs ones calculated in [10], by using recent Padova isochrones and atmospheres models, (including spectra for massive stars and planetary nebulae from [16] and [13]), for six

metallicities (Z= 0.0001, 0.004, 0.004, 0.008, 0.02 and 0.05) and ages from $\tau = 0.1$ Myr and 15 Gyr

In Fig. 2 we show the spectral energy distributions (SEDs) corresponding to these same extreme 4 models as labelled. These SEDs have been computed by using the information proceeding from the star formation and metal enrichement histories shown in Fig. 1. Once these SEDs calculated, and using the filters curves, it is easy to compute magnitudes and colors in the the Johnson or SDSS systems, We give colors B-V and V-K and magnitude M_B for each galaxy in this same figure. As expected colors are bluer when the galaxy mass is smaller and/or when the efficiency index N is higher.

4 The modeled redshift evolution of the metallicity-luminosity relation

Finally, once the photometric and the chemical evolution models computed, we may represent the metallicity-magnitud relation for different times or, equivalently, different redshift. We show this relation for $z = 0.0, 2.5$ and 4.5 from top to medium and bottom panels, respectively, in Fig. 3.

In the top panel the local M_B-O/H relation is plotted. There we have the whole 440 results of our grid of models as open squares. The full (red) dots give the results for 7 selected models representing the diagonal line in our plane of models, that is, galaxies in the Hubble Sequence. The local data from [12, 7, 15, 17] are represented

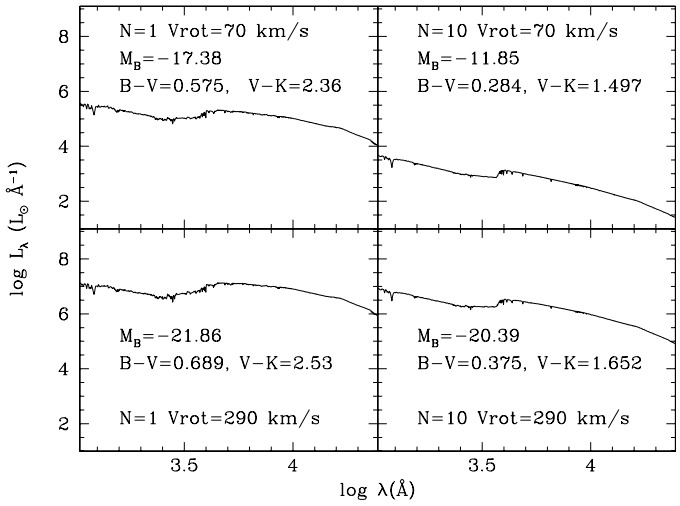

Fig. 2 The spectral energy distribution (SEDs) for the same 4 extreme models shown in Fig. 1.

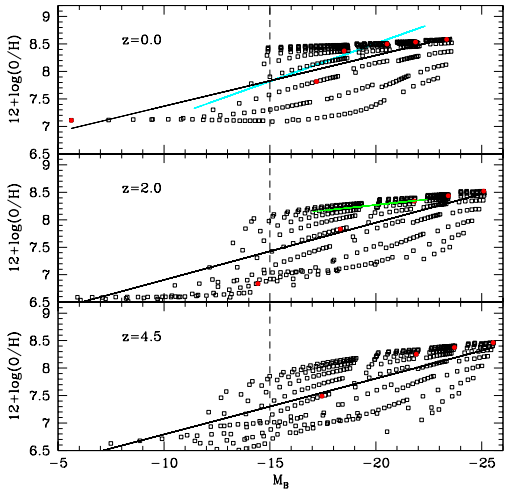

Fig. 3 The metallicity-magnitud relation for three redshifts z=0, 2 and 4.5. The open squares are the model results and the solid black line is the fit to these models. The data are represented by the dashed lines.

by the cyan line which is a least squares straighth line for the whole set of data of all authors. The solid black line is the equivalent line for our models. We see that both lines are very similar.In the medium panel we show the same relation for z=2.5. There we shown as a green line a similar least squares straighth line obtained with data from [5, 8, 6] for objects located at redshift $0.2 < z < 1.2$. It is clear that this sample of objects show a selection effect since only the brightnest and evolved theoretical galaxies of our grid fall in the observational region.

The relation obtained with our theoretical models has a similar slope in the three panels, as it is demostrated by the solid line fitting our models. However, the highest the redshift, the lowest the abundance for a same value of magnitud $M_B = -15$, marked by the short-dashed line: the oxygen abundance $12 + \log(O/H) \sim 8$ for z=0.0 and only 7.5 for Z= 4.5.

The dispersion of data is much smaller for observations than for our models. There is two possible explanations:1) theoretical models are representing in some cases inexistent galaxies; or 2) there is an observational selection effect which eliminates the low surface brighness and/or other dwarf galaxies of the data samples. We think that this second possibility is probable since there is a set of data from [14] for Ultraluminous Infrared galaxies at redshift z$\sim$ 0.1, which doesn't show any relation at all, such as we show in 4, and which are, however, well reproduced by the models. Following our grid, these galaxies are massive but the molecular cloud and the star formation efficiencies are very variable among them, thus, producing very different oxygen abundances with similar values of luminosities in band K.

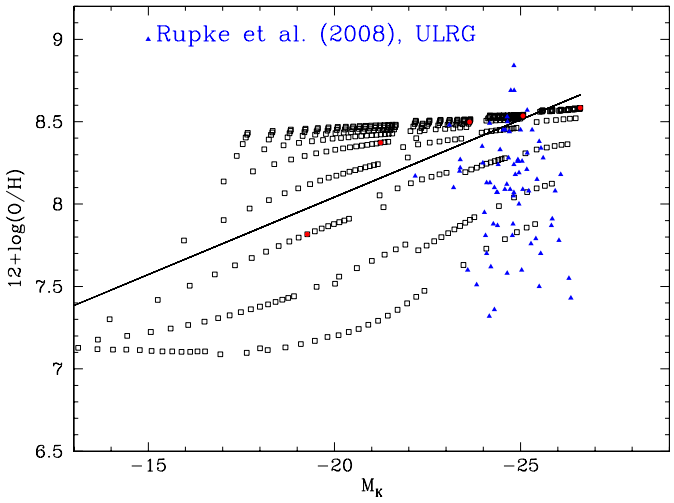

Fig. 4 The metallicity-magnitud relation in K-band for redshift zero for our grid of models compared with the data from [14] for Ultraluminous Infrared galaxies, shown as full blue triangles

References

1. Ferrini F., Matteucci F., Pardi C., Penco U., 1992, ApJ, 387, 138
2. Ferrini F.,Mollá M., Pardi M. C., Díaz A. I., 1994, ApJ, 427, 745
3. Gavilán M., Buell J. F., Mollá M., 2005, A&A, 432, 861
4. Gavilán M., Mollá M., Buell J. F., 2006, A&A, 450, 509
5. Kobulnicky, H. A., et al. 2003, ApJ, 599, 1006
6. Lamareille, F., Contini, T., Brinchmann, J., Le Borgne, J.-F., Charlot, S., & Richard, J. 2006, A&A, 448,
7. Lee, J. C., Salzer, J. J., & Melbourne, J. 2004, ApJ, 616, 752
8. Liang, Y. C., Hammer, F., Flores, H., Elbaz, D., Marcillac, D., & Cesarsky, C. J. 2004, A&A, 423, 867
9. Mollá, M., Díaz A. I., 2005, MNRAS, 358,521M
10. Mollá M., García-Vargas M. L., Bressan A., 2008, MNRAS, in preparation, Paper I
11. Mollá M., Díaz A. I., 2008, MNRAS, in preparation
12. Pilyugin, L. S., Vílchez, J. M., & Contini, T. 2004, A&A, 425, 849
13. Rauch T., 2003, A&A, 403, 709
14. Rupke, D. S. N., Veilleux, S., & Baker, A. J. 2008, ApJ, 674, 172
15. Salzer, J. J., Lee, J. C., Melbourne, J., Hinz, J. L., Alonso-Herrero, A., & Jangren, A. 2005, ApJ, 624, 661
16. Smith L. J., Norris R. P. F., Crowther P. A., 2002, MNRAS, 337, 1309
17. van Zee, L., & Haynes, M. P. 2006, ApJ, 636, 214